Tunnelling and Underground Space Technology 131 (2023) 104776

Contents lists available at ScienceDirect

Tunnelling and Underground Space Technology incorporating Trenchless Technology Research

journal homepage: www.elsevier.com/locate/tust

A study of the critical velocity and the confinement velocity of fire accident in a longitudinally ventilated underground train with different door opening scenarios

Zhihe Su [a], Yanfeng Li [a,*], Shan Feng [b], Hua Zhong [c,*], Junmei Li [a], Wenbo Liu [a], Chao Chen [a], Jiaxin Li [a]

[a] Beijing Key Laboratory of Green Built Environment and Energy Efficient Technology, Beijing University of Technology Beijing, China
[b] China University of Political Science and Law, China
[c] School of Architecture, Design and Built Environment, Nottingham Trent University, Nottingham NG1 4FQ, United Kingdom

ARTICLE INFO

Keywords:
Fire
Underground tunnel
Critical velocity
Confinement velocity
Door opening scenarios

ABSTRACT

The critical velocity, confinement velocity and smoke back-layering length are significant factors for smoke control in a tunnel fire. This research aims to analysis the correlation of these 3 key smoke control parameters in the different door opening scenarios during a fire in the metro train carriage that stopped in the tunnel. Scaled model experiment measurement and numerical simulations were carried out for the propagation and control of smoke. Five fire locations in the train and two side doors opening scenarios of the train were considered. Results show that smoke back-layering length in the train can be barely influenced by the activation time of the longitudinal ventilation system. However, the opening of side doors could result in a shorter smoke back-layering length in the train. Furthermore, we present a dimensionless correlation for the critical velocity and confinement velocity of underground train fires caused by fires in the double-length narrow space of an underground tunnel. This study provides a predictive model for the design of smoke control systems for fire of train stopped in underground tunnels.

1. Introduction

With the acceleration of urbanization and the continuous improvement of infrastructure, underground transport has developed rapidly (Feng et al., 2020). In the long and narrow underground tunnels, once an underground train fire occurred, it could result in devastating repercussions. (Li et al., 2018). Fire accidents have happened around the world including the Baku underground fire in Azerbaijan, which caused 558 deaths and 269 injuries (1995), the Daegu underground fire in South Korea, which caused 192 deaths and 151 injuries (2003), and the Moscow underground fire that caused more than 40 people died and more than 100 injuries (2004), and 18 people were injured in a Hong Kong underground arson incident (2017) (Peng et al., 2019; Zhang et al., 2016; Zhao et al., 2018). According to statistics, most deaths are caused by smoke gas during the fire. Hence, it is of great significance to get smoke control during the fire in the underground tunnel and train for safe evacuation and reducing casualties.

Longitudinal ventilation is an important method for confining upstream smoke diffusion. A large number of studies have been conducted on the smoke flow characteristics in longitudinal ventilation tunnels. Based on the theoretical model, Thomas (1958) firstly proposed an equation to predict the back-layering length in an ordinary tunnel by analyzing the Froude number. Oka and Atkinson (1995); (Wu and Bakar, 2000) conducted small-scale tunnel model tests and proposed a dimensionless prediction model between the dimensionless heat release rate (HRR) and the critical velocity. Combining the dimensionless analysis with the small-scale experiments, Ying et al. (2011) presented correlations between smoke back-layering length, dimensionless heat release rate, and dimensionless longitudinal ventilation velocity and found that the maximum dimensionless HRR is 0.15.

Recently, many researchers have studied the critical velocity and the smoke back-layering length under different fire scenarios in the longitudinal ventilation tunnel. From the tunnel structure perspective, the influence of tunnel slope (Du et al., 2018; Ko et al., 2010; Li et al., 2019), the influence of cross-sectional geometry (Li and Ingason, 2017; Weng et al., 2015), and the influence of bifurcation angle (Huang et al., 2020) in the smoke back-layering length and critical velocity were studied.

* Corresponding authors at: Beijing University of Technology, Beijing 100124, China.
E-mail addresses: liyanfeng@bjut.edu.cn (Y. Li), hua.zhong@ntu.ac.uk (H. Zhong).

https://doi.org/10.1016/j.tust.2022.104776
Received 11 July 2022; Received in revised form 27 August 2022; Accepted 26 September 2022
Available online 18 October 2022

Nomenclature

Q	heat release rate (kW)
$Q*$	dimensionless heat release rate
L	smoke back-layering length (m)
m_b	the airflow through the train blockage region (kg)
L_f	the distance between the fire source and the front of the train (m)
g	gravitational acceleration (m/s^2)
m_t	the airflow impacting the front of the train (kg)
m_l	the airflow generated by the longitudinal ventilation (kg)
m_e	the airflow through the emergency evacuation door (kg)
V_c*	dimensionless critical velocity
m_{in}	the airflow reach the train (kg)
$V_{in\text{-}conf}$	confinement train ventilation velocity (m/s)
$V_{in}*$	dimensionless train ventilation velocity
$V_{conf}*$	dimensionless confinement velocity
c_p	The specific heat capacity of air (kJ/kg·K)
$\overline{H}$	hydraulic diameter (m)
V_c	critical velocity (m/s)
T_0	ambient temperature (K)
u_0	ambient velocity (m/s)
$L*$	dimensionless smoke back-layering length (m)
$X*$	dimensionless fire source location
D	fire source diameter (m)
$V_{in\text{-}c}$	critical train ventilation velocity (m/s)
V_l	longitudinal ventilation velocity (m/s)

Greek letters

ρ_∞	ambient density (kg/m^3)

Subscripts and subscripts

*	dimensionless expression
in	train
c	critical condition
conf	confinement condition

Considering the effect of ventilation modes on the smoke back-layering length, including natural ventilation through the shaft (Yan et al., 2016; Yao et al., 2016), and semi-transverse ventilation (Zhou et al., 2019). For vehicle blockage fire scenarios, Zhang et al. (2016) numerically studied the smoke back-layering length in an underground tunnel with different train lengths and longitudinal ventilation velocities. Hu et al. (2020) investigated the critical velocity and transition velocity caused by a train fire in an underground tunnel and obtained the piecewise relationship between dimensionless smoke back-layering length and dimensionless longitudinal ventilation velocity for train fires in ventilation tunnels. Zhu et al. (2017) studied the critical velocity and back-layering length by combining the blockage and slope. Tang et al. (2013) carried out a series of tests to investigate the influence of a vehicle obstruction on the back-layering length and critical velocity in a longitudinal ventilated tunnel, and they also provided a formula to predict the back-layering length and critical velocity. Jiang et al. (2018) conducted a series of scaled experiments by considering the influence of blocking factors such as the blocking ratio, blocking direction, and blocking-fire distance on the critical ventilation speed. Shafee et al. (2018) investigated smoke flow while accounting for vehicle obstruction and tunnel inclination. Table 1 summarises the key prediction models proposed or modified in the preceding literature.

The above literature review considered actual factors that affect critical velocity and smoke back-layering length for smoke confinement. However, there are two research gaps in the underground train fire scenario that still lack the study. First, all of the preceding studies only addressed one long and narrow space, but an underground tunnel fire may occur within a train that has stopped in a tunnel which should be considered as a double long-narrow space fire since both the train's inner space and the space between the train and the inner wall of the tunnel are long and narrow. Second, only one side door is considered in prior research, and the effects of the side door superposition effect on smoke flow are frequently overlooked. Furthermore, How the emergency evacuation doors and side doors of underground trains open are different from how they open in ordinary single tunnels. The mode of cooperation of the doors inevitably influences the ventilation air velocity in the train and the smoke propagation. This research aims to account for different door opening scenarios and the superposition impact of side doors optimizing the prediction model of the critical velocity and the smoke back-layering length for trains stopped in underground tunnels during a fire.

Table 1
Main prediction model for critical velocity and smoke back-layering length.

References	The proposed or modified model
(Wu and Bakar, 2000)	$V_c^* = \begin{cases} 0.81Q^{*1/3} & Q^* \leqslant 0.20 \\ 0.4 & Q^* > 0.20 \end{cases}$
(Ying et al., 2011)	$V_c^* = \begin{cases} 0.81Q^{*1/3} & Q^* \leqslant 0.15 \\ 0.43 & Q^* > 0.15 \end{cases}$
(Zhu et al., 2017)	$V_c^* = (1-\phi)(1+2.75\beta)0.9Q^{*1/3}$
(Hu et al., 2020)	$V_c^* = \begin{cases} 1.04\dot{Q}_e^{*1/3}, & \dot{Q}_e'' \leqslant 0.12 \\ 0.51, & \dot{Q}_e^* > 0.12 \end{cases}$

Under longitudinal ventilation, smoke would diffuse upstream of the fire source, when the buoyancy force is greater than the inertial force. The smoke front would come to a halt until the buoyancy and inertial force were balanced. As shown in Fig. 1, a back-layering length of L exists between this point and the fire source. The L can be considered as having three situations: (a) $L = 0$; (b) $L = L_f$; (c) $L \geq L_f$. Smoke is controlled downstream of the fire source when the longitudinal ventilation is quite large. Then, the smoke will spread upstream along the train if the longitudinal ventilation velocity is less than the critical velocity. As a further movement, the smoke will overflow the train and continue to spread upstream.

For smoke control in tunnel fire accidents, the ventilation mode with the confinement velocity would be a feasible or alternative ventilation mode, which firstly was defined by Vauquelin and Telle (2005). Vauquelin and Telle (2005) conducted experiments to study the smoke backflow behavior in tunnel fires, and they found that when L/H is less than 4., the smoke layer length is not very sensitive to variations in the extraction flow rate. It can be considered that the smoke flow downstream from the vent is completely controlled and confined. The longitudinal ventilation velocity at this time they called the "confinement velocity". Compared with Vauquelin and Telle (2005b), for the double long-narrow space, the longitudinal ventilation velocity which can control the smoke back layering length at the confinement point ($L = L_f$) is defined as the confinement velocity in this study, as shown in Fig. 1 (b). This study aims to establish the expression for the critical velocity and the confinement velocity induced by train fire in a double long-narrow space, which can be anticipated by assuming zero and L_f for the smoke back-layering lengths, respectively (Liu et al., 2020).

2. Theoretical model

2.1. The smoke back-layering length under side door-closed condition

The airflow impacting process at the front of the train is shown in

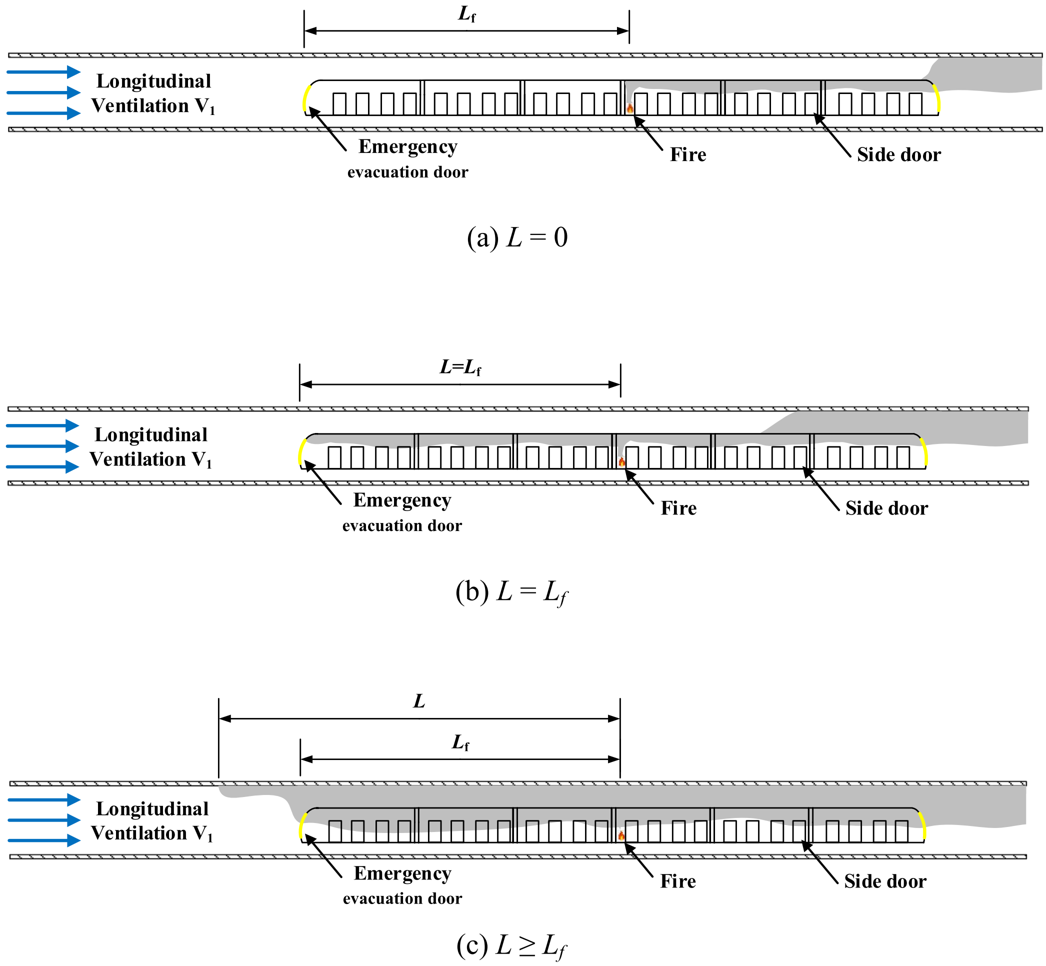

Fig. 1. The schematic diagram of smoke back-layering in the underground tunnel.

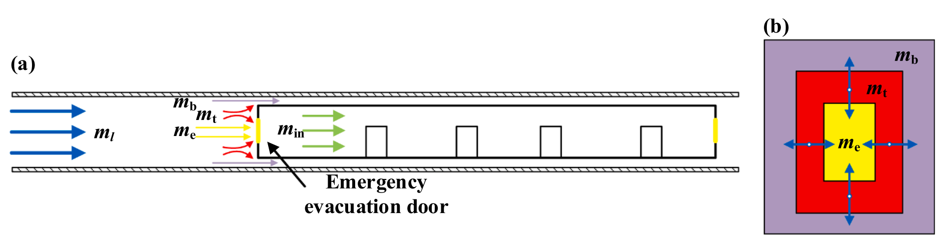

Fig. 2. The incoming air impacts the process at the front of the train.

Fig. 2. Under longitudinal ventilation surroundings, the incoming air is divided into three parts at the front of the train. As shown in the figure, m_l is the airflow generated by the longitudinal ventilation, m_e is the airflow through the emergency evacuation door, m_b is the airflow through the train blockage region, m_t is the airflow impacting the front of the train, m_{in} is the airflow reach the train. Due to the general mass conservation relationship in fluid mechanics, the mass flux (m) in a stream tube with a single exit and inlet remains constant throughout time. As a result of the correlation between these variables, we get the following:

$$m_l = m_e + m_b + m_t \tag{1}$$

$$m_l = \rho A_l V_l \tag{2}$$

$$m_e = \rho A_e V_l \tag{3}$$

$$m_b = \rho(1-\varphi)A_l V_l \tag{4}$$

$$m_t = \rho(\varphi A_l - A_e)V_l \tag{5}$$

Where A_l is the area of the tunnel, A_e is the area of the emergency evacuation door, φ is the train blockage ratio, and V_l is the longitudinal ventilation velocity. In this study, the airflow, which impacts the front of the train, is assumed uniformly scattered into two parts, one part reaches the train through the emergency evacuation door, and the other part enters the train blockage region, due to the air direction is perpendicular to the front of the train.

$$m_{in} = m_e + \frac{m_t}{2} \tag{6}$$

Due to the closing of the side doors, the flow in the trains would not be affected by the side doors, and a stable flow would be formed in the train. The ventilation velocity in the train can be calculated as follows:

$$V_{in} = \frac{m_{in}}{\rho\varphi A_l} \tag{7}$$

Substituting Eqs. (3), (5), (6) into Eq. (7), the expression of the velocity in the train and the longitudinal ventilation velocity can be deduced as follows:

$$V_{in} = \frac{V_l}{2}\left(\frac{A_e}{\varphi A_l}+1\right) \tag{8}$$

$$V_{in}^* = \frac{V_l^*}{2}\sqrt{\frac{\overline{H}_{tunnel}}{\overline{H}_{train}}}\left(\frac{A_e}{\varphi A_l}+1\right) \tag{9}$$

Eq. (9) determined the basic relationship between the train ventilation velocity and the longitudinal ventilation velocity, but its accuracy still needs further consideration. When the side doors are closed, double long-narrow space is formed in the tunnel and the train. In this condition, the train may be thought of as a regular tunnel with a single exit and inlet. The previous study (Thomas, 1958; Ying et al., 2011) found the following relationship between dimensionless smoke back-layering length, heat release rate, and train ventilation velocity in a side door-closed train:

$$l^* = \frac{L}{\overline{H}_{train}} \propto \ln\left(\frac{Q^{*1/3}}{V_{in}^*}\right) \tag{10}$$

where $l^* = L/\overline{H}_{train}$- the dimensionless back-layering length,

$Q^* = Q/\rho_0 c_p T_0 g^{1/2}\overline{H}_{train}^{5/2}$- the dimensionless heat release rate,

$V_{in}^* = V_{in}/\sqrt{g\overline{H}_{\text{train}}}$- the dimensionless ventilation velocity in the train.

2.2. The smoke back-layering length under side door-opened condition

Eq. (10) provides the essential relationship between the back-layering length, the heat release rate and the longitudinal ventilation velocity when the side doors are closed. However, consideration needs to be given to what effect the side door has on the fire in the trains. The side doors' cooperation mode affects the stratification and entrainment of air within the train, which results in a change in ventilation velocity in the tunnel necessary to overcome the smoke buoyancy force. In addition, the influence of the side doors is often combined with the location of the fire source, which will produce different smoke movement processes (Cong et al., 2020).

Therefore, the present work uses the dimensionless fire location, X^*, to replace the distance between the fire source and the front of the train, L_f. The dimensionless fire location, X^*, is defined as the ratio of the distance between the fire source and the front of the train to the train length:

$$X^* = \frac{L_f}{L_{train}} \tag{11}$$

Cong et al. (2020) have also investigated the influence of the fire located on the heat flow rate of the side doors. Under the heat release rate is 5 MW, the maximum heat flow rate of the side door near the fire is only 0.15 MW, with the natural ventilation in the tunnel. Moreover, the air velocity in the train is less than in the blockage region, due to the emergency evacuation door being smaller than the blockage area. Therefore, we can deduce that the smoke in the blockage region will not diffuse upstream when the air velocity in the train reaches the critical velocity.

According to Eq. (12) and mentioned above, the smoke back-layering length (L) is affected by the heat release rate (Q), dimensionless fire location (X^*), longitudinal ventilation velocity (V_l), the hydraulic diameter of the train ($\overline{H}_{\text{train}}$), air density ($\rho_0$), ambient temperature ($T_0$), thermal capacity of air (c_p), and gravitational acceleration (g) while the fire occurs in the train and the side doors are opened. As a result, the smoke back-layering length can be expressed as follows:

$$f\left(L, \overline{H}_{\text{train}}, Q, V_l, c_p, \rho_0, T_0, g, X^*\right) = 0 \tag{12}$$

Ji et al. (2012) believe that the variables without any connection are the independent variables to be studied. Therefore, specify the$\overline{H}_{\text{train}}$, V_1, c_p, and ρ_0 as the independent variables, then Eq. (12) can be rearranged as:

$$f\left(\frac{L}{\overline{H}_{\text{train}}}, \frac{Q}{\overline{H}_{\text{train}}^2 V_l^3 \rho_0}, \frac{c_p T_0}{V_l^2}, \frac{g\overline{H}_{\text{train}}}{V_l^2}, X^*\right) = 0 \tag{13}$$

Subsequently, the smoke back-layering length in the underground train can be derived as:

$$\begin{aligned} \frac{L}{\overline{H}_{\text{train}}} &= f\left(\frac{Q}{\overline{H}_{\text{train}}^2 V_l^3 \rho_0}, \frac{c_p T_0}{V_l^2}, \frac{g\overline{H}_{\text{train}}}{V_l^2}, X^*\right) \\ &= f\left(\frac{gQ}{\rho_0 c_p T_0 \overline{H}_{\text{train}} V_l^3}, X^*\right) \\ &= f\left(\frac{Q}{\rho_0 c_p T_0 g^{1/2}\overline{H}_{\text{train}}^{5/2}} \Big/ \left(\frac{V_l}{\sqrt{g\overline{H}_{\text{train}}}}\right)^3, X^*\right) \\ &= f\left(\sqrt{\frac{\overline{H}_{\text{train}}}{\overline{H}_{\text{tunnel}}}}\left(\frac{Q}{\rho_0 c_p T_0 g^{1/2}\overline{H}_{\text{train}}^{5/2}}\right)^{1/3} \Big/ \left(\frac{V_l}{\sqrt{g\overline{H}_{\text{tunnel}}}}\right), X^*\right) \end{aligned} \tag{14}$$

Substituting the dimensionless longitudinal ventilation velocity V^*, and dimensionless heat release rate Q^* in Eq. (14), the expression of the dimensionless smoke back-layering length in the underground train is obtained:

$$L^* = f\left(\sqrt{\frac{\overline{H}_{\text{train}}}{\overline{H}_{\text{tunnel}}}}\frac{Q^{*1/3}}{V_l^*}, X^*\right) = f\left(\frac{Q^{*1/3}}{V_l^*}, X^*\right) \tag{15}$$

where $V_l^* = V_l/\sqrt{g\overline{H}_{\text{tunnel}}}$ is the dimensionless ventilation velocity in the tunnel.

3. Experiments

3.1. Experimental setups and test conditions

To investigate the critical velocity and confinement velocity, a small-scale tunnel with an underground train (1:15) was built using the Froude scaling method. Fig. 3 shows the schematical experimental setups and measurement apparatus. The total length of the scaled tunnel is 20 m long, 0.675 m wide, and 0.5 m high, representing the full-scale tunnel is 300 m long, 10.125 m wide, and 7.5 m high. Different from the common shield tunnel at present, the experimental platform is designed according to the space dimension of the early Beijing subway tunnel. The size of the model train is 120 cm long, 32.8 cm wide, and 24.6 cm high. Also, the train have six side doors (8 cm wide and 9.8 cm high) with a spacing of 12 cm and two emergency evacuation doors (15.7 cm wide and 8.2 cm high). The rectangular wall of the tunnel is made of 5 mm thick iron, and one sidewall is made of reinforced transparent glass.

Methane was chosen as the fire source's fuel in this research, and the mass flow rate of methane is used to determine the heat rate of fire. In this study, four heat release rates (3 kW, 4 kW, 5 kW, 6 kW) were used in the experiment. Based on the Froude model similarity criterion, the equivalent maximum heat release rate of the experimental design is about 5.2 MW. According to the Code for design of metro (GB50157-2013) of Chinese Mainland, the train fire is designed as 5MW. At the same time, in order to compare the smoke control laws under different fire HRR conditions, we selected different fire HRRs near 5MW. The train is located in the tunnel's center, and K-type sheathed thermocouples with a 4 cm spacing were installed 1 cm below the train ceiling. Throughout the experiment, 30 K-type thermocouples (diameter: 1 mm) were used. Their precision and reaction time are 0.1 °C and 1 s, respectively. A mechanical fan producing longitudinal ventilation was installed at the end of the tunnel. The ventilation velocity was controlled

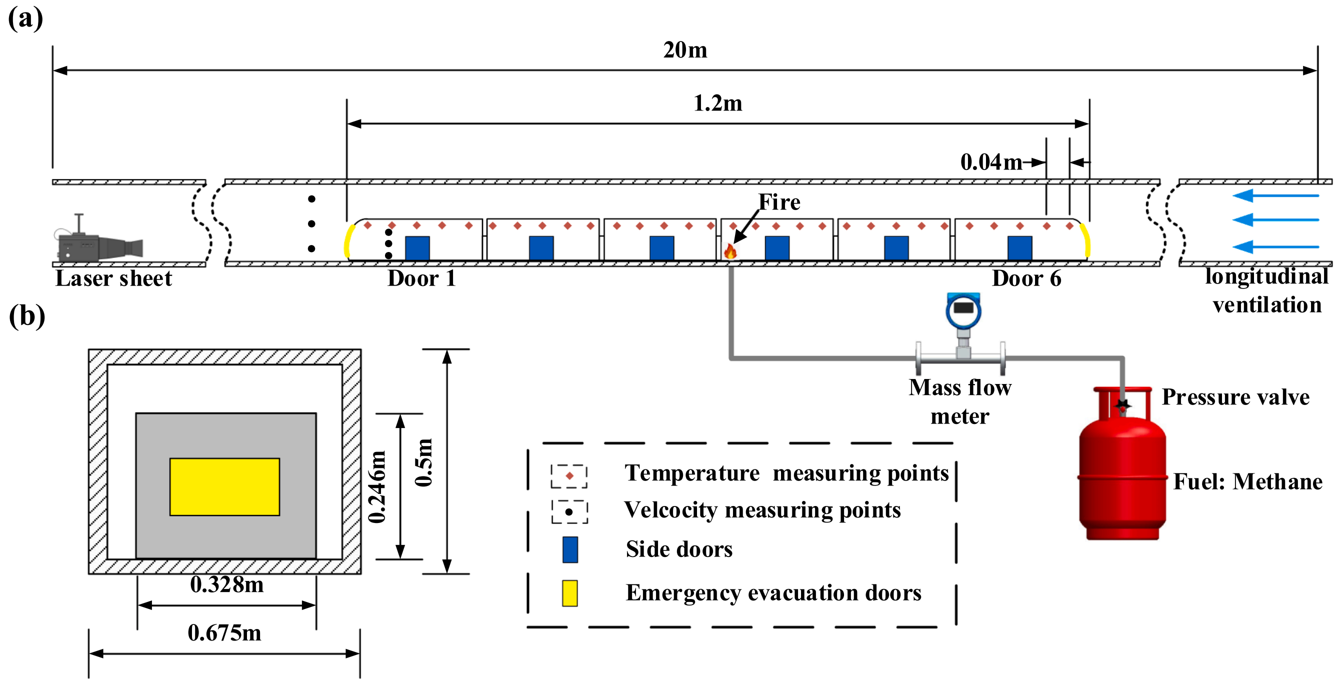

Fig. 3. Schematic of the experimental setup.

by altering the fan's flow rate. Two grid baffles were installed near upstream portal to provide steady wind velocity. The longitudinal ventilation velocity was measured in real time by hot-wire anemometers. Nine velocity measurement points are evenly placed on the cross-section of the tunnel and train. The values of the longitudinal ventilation velocity and the train ventilation velocity are obtained by taking the average value of nine measurement points, respectively. The photo of the tunnel and underground is shown in Fig. 4. A total of 24 tests were conducted to obtain the critical velocity and confinement velocity under different fire heat release rates and longitudinal ventilation velocities in the tunnel. In Tests 1–8, the relationship between the train ventilation velocity and the longitudinal ventilation velocity was obtained through the velocity tests under the fireless condition. The experimental conditions are summarized in Table 2.

Table 2
Experimental conditions.

Test no.	Description	Fire heat release rate (kW)	V_l (m/s)	X^*
1–16	Side door-closed	0	0.72, 0.77, 0.83, 0.88, 0.93, 0.98, 1.03, 1.08	0.5
		3	0.62, 1.08	
		4	0.62, 1.11	
		5	0.71, 1.15	
		6	0.75, 1.18	
17–24	Side door-opened	3	0.38, 0.74	0.5
		4	0.40, 0.72	
		5	0.52, 0.78	
		6	0.55, 0.83	

3.2. Experimental results and analysis

Fig. 5 presents the variation of the ventilation velocity in the train with different longitudinal ventilation velocities. the results showing the train ventilation with the longitudinal ventilation is a linear correlation, which also agrees with Eq. (8) qualitatively. The train ventilation

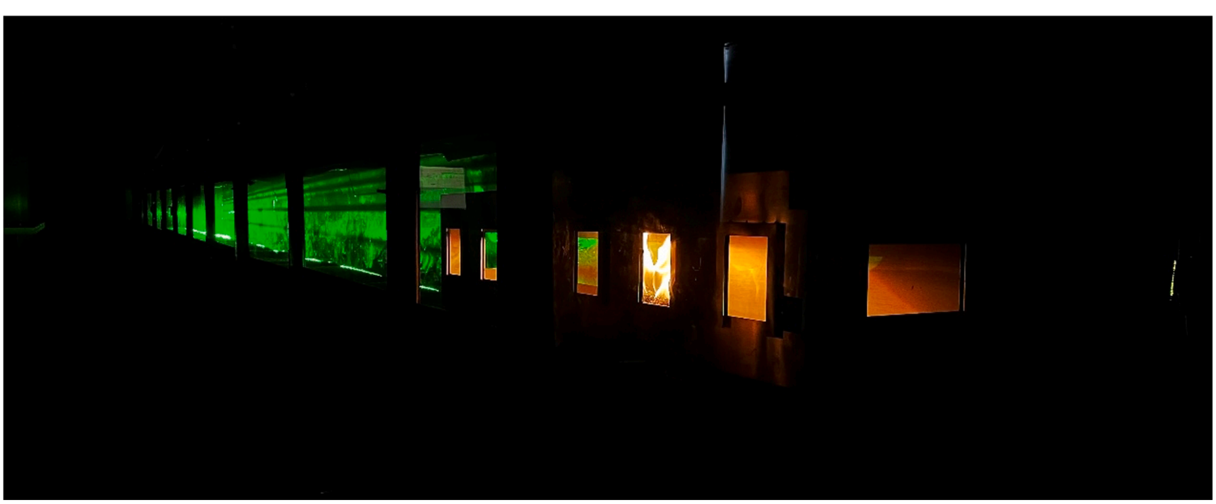

Fig. 4. The photo of the 1:15 experimental model.

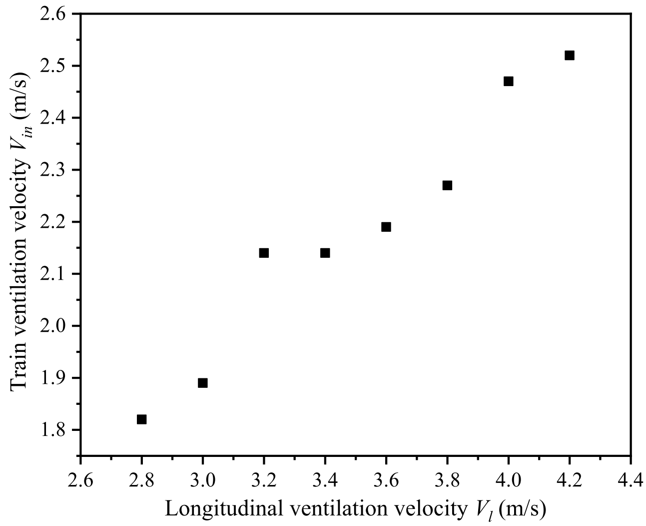

Fig. 5. The variation of the train ventilation velocity with different longitudinal ventilation velocities.

velocity while the longitudinal ventilation velocity increases.

Fig. 6 shows the required critical velocity and confinement velocity with different door opening ways. As can be seen from the result, the critical velocity and confinement velocity for smoke control varies depending on how the train side doors are opened. First of all, the confinement velocity is smaller than the critical velocity because of the addition of smoke back-layering length. Besides, compared with the case where the train side doors are closed. The opening of the side doors facilitates smoke evacuation from the train and, in addition, the critical velocity and confinement velocity for smoke control is reduced. Based on the results, these experimentally variations of the train ventilation velocity with different longitudinal ventilation velocities can be compared with simulation results with the theoretical models to verify the accuracy.

4. Numerical simulation

4.1. Physical model and boundary conditions

The Fire Dynamic Simulator (FDS) version 6.6 was used in this study to examine smoke diffusion in the event of a train fire due to interactions between smoke buoyancy and the inertial force of airflow. A description of the model, many validation examples, and reports can be found on https://fire.nist.gov/fds/(Ji et al., 2013).

The numerical model consists of a 500 m long tunnel and an underground train consists of 6 compartments; Fig. 7 provides a schematic diagram of the FDS model. Each train is 20 m long, 2.8 m wide, and 3.8 m high. The tunnel model in this research is a rectangular section tunnel of 500 m in length, 4.8 m in width, and 5.2 m in height, based on the aspect ratio of real tunnels. The effective clearance area of the tunnel is 24.96 m^2, and the blocking rate is 0.43. The materials used to build tunnels and underground surfaces such as walls, floors, and ceilings are listed in Table 3. The tunnel's left portal is set up as an air "SUPPLY" vent to accomplish longitudinal ventilation at various velocities, and the right portal is set as "OPEN." The door is set to "Deactivate" when the door is closed. In this simulation, the default heat transfer technique is used. A cuboid fire source is specified as a "BURNER" with dimensions of 2 m (length), 1.8 m (width), and 0.2 m (height) that is positioned in the middle of the train floor. The fire source is given a heat release rate per unit area (HRRPUA). The starting ambient temperature in all simulations is 293.15 K, with an initial pressure of 101.325 kPa.

4.2. Simulated conditions

The flame retardant materials are commonly applied in current underground trains, which may substantially limit the size of a train fire, According to the results of related fire experiments (Marková et al., 2020), the size of fire caused by luggage in the train is generally 2 MW. However, as the fire develops and expands, the heat release rate will further increase. Therefore, the fire sources with heat release rates of 2, 3, 4, and 5 MW were selected to represent the unfavorable scenarios. Besides, the longitudinal ventilation is activated 120 s after the fire to ensure the evacuation of people downstream. T-Square fire was adopted

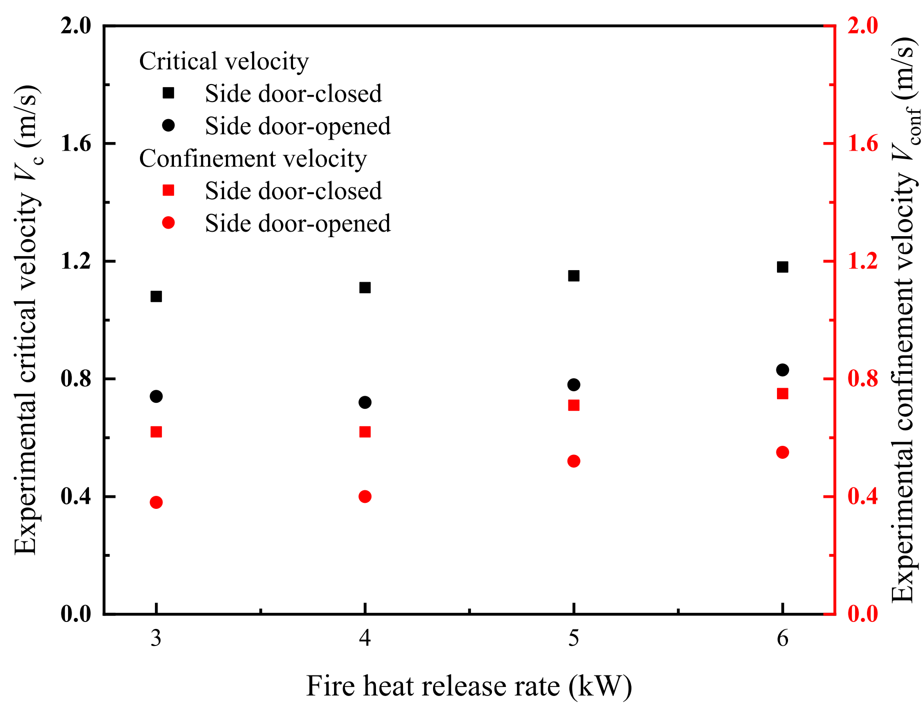

Fig. 6. The critical velocities and the confinement velocities from the experiments.

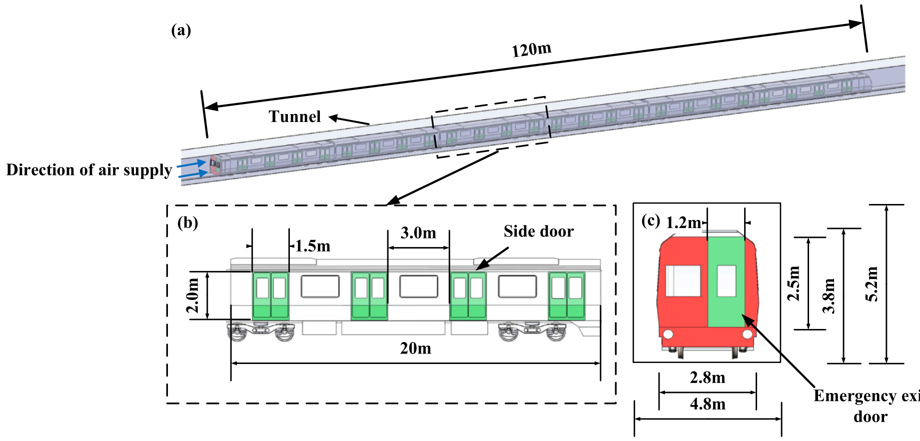

Fig. 7. The schematic diagram of the model.

Table 3
The thermal properties of the material.

Model	Material	Density (kg/m^3)	Species heat (kJ/(kg·K))	Thickness (m)	Conductivity (W/m·K)
Tunnel Surfaces	Concrete	2280	1.04	0.3	1.80
Train Surfaces	Steel	7850	0.46	0.1	45.8

for the fire growth in this simulation. The whole simulation time is 1000s, ensuring that the smoke movement is in the quasi-steady state.

A total of 216 simulation scenarios were operated to account for the impacts of the aforementioned door opening, fire heat release rate, longitudinal ventilation velocity, and fire location. Table 4 summarizes the scenarios. Among them, the fire scenarios of cases 1–32 simulated the effect of various longitudinal ventilation velocities on the smoke back-layering length under the side door-closed condition. Subsequently, cases 33–64 compared the influence of the longitudinal ventilation activated time on the smoke back-layering length. Finally, cases 65–216 simulated fire situations with various fire locations and longitudinal ventilation velocities under the side door-opened condition. A set of horizontal thermocouples spaced 1 m apart were installed 0.05 m below the train ceiling. At the cross-sectional position 1 m away from the front of the train, 9 velocity measuring points are evenly arranged to measure the train ventilation velocity.

Table 4
Detail simulation cases for train fire.

Description	Simulation case	Fire heat release rate (MW)	V_l (m/s)	X^*	longitudinal ventilation acvitation time (s)
Side door closed	1–32	2, 3, 4, 5	2.8, 3.0, 3.2, 3.4, 3.6, 3.8, 4.0, 4.2	0.5	120
	33–64	2, 3, 4, 5	2.8, 3.0, 3.2, 3.4, 3.6, 3.8, 4.0, 4.2	0.5	0
Side door opened	65–96	2, 3, 4, 5	2.4, 2.6, 2.8, 3.0, 3.1, 3.3, 3.5, 3.7	0.17	120
	97–132	2, 3, 4, 5	2.0, 2.2, 2.4, 2.6, 2.7, 2.8, 2.9, 3.0, 3.1	0.33	120
	133–156	2, 3, 4, 5	2.1, 2.3, 2.5, 2.8, 3.0, 3.1	0.5	120
	157–184	2, 3, 4, 5	1.8, 2.0, 2.2, 2.4, 2.6, 2.8, 3.0	0.67	120
	185–216	2, 3, 4, 5	1.8, 2.0, 2.2, 2.4, 2.6, 2.8, 3.0, 3.2	0.83	120

4.3. Mesh size sensitivity analysis

Although FDS is extensively used in fire calculations, engineers must grasp the calculation concepts underlying it to pick acceptable calculation parameters. Before doing numerical calculations, it is vital to assess the mesh grid size sensitivity; a good grid size may considerably cut calculation time while assuring calculation accuracy. According to the grid resolution requirements in the FDS user's guide (Mcgrattan et al., 2010), the fire simulation results are relatively accurate when the ratio of the grid size d to the dimensionless fire source characteristic diameter D^* is kept in a range of 4 –16. At the same time, the numerical simulation results of the fire scene are closer to the actual situation when the grid size is $0.1D^*$. Determine the size of the characteristic diameter of the fire source according to Eq. (16). The selected grid sizes are respectively 0.16, 0.18, 0.20, and 0.24 when the fire source power is 5 MW and the

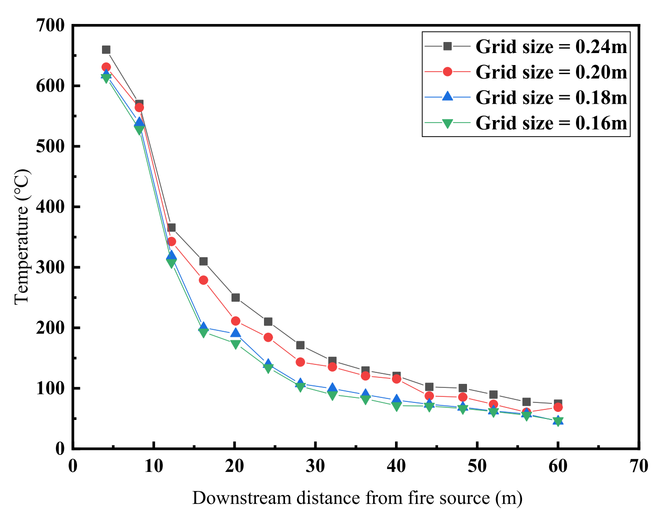

Fig. 8. Grid independence verification.

characteristic diameter is 1.8 m.

Fig. 8 shows the mesh grid size sensitivity analysis for the four grid sizes. 15 temperature measurement points with different grid sizes in the area near the fire source (60 m downstream of the fire source) were compared under the condition of no mechanical ventilation. Results show that the longitudinal temperature distribution in the tunnel differs slightly when the mesh size is less than 0.18. Taking into account the requirement to save calculation time, the grid size used in this study is 0.18 m.

$$D^* = \left(\frac{\dot{Q}}{\rho_\infty c_p T_\infty \sqrt{g}}\right)^{\frac{2}{5}} \tag{16}$$

4.4. Model validation

The feasibility of FDS to simulate the tunnel fire has been extensively validated by the experiment and theory models. The FDS predicted train ventilation velocity has been compared with the scale experimental results and those predicted based on Eq. (11), shown in Fig. 9. The figure implies that the numerical results predicted by FDS were in good agreement with those obtained from the experiments and the theoretical values; this further verified the applicability of the Eq. (9) to calculate the train ventilation velocity under longitudinal ventilation surroundings.

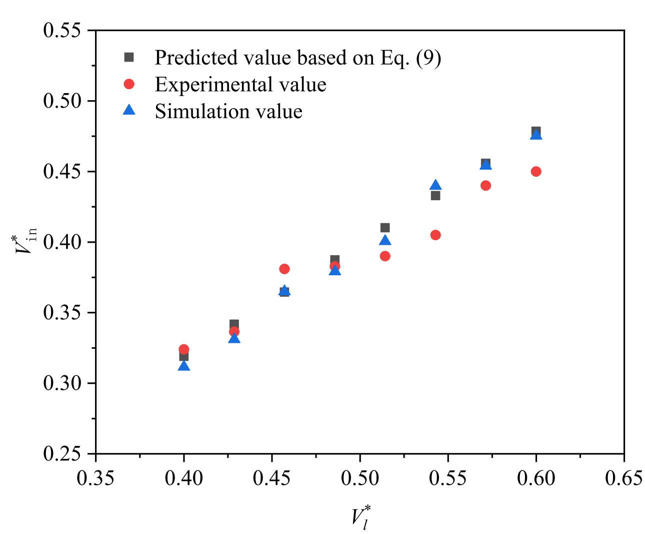

Fig. 9. Relationship between V_l* and V_{in}* from the experiments, simulation, and the theoretical value.

5. Results and discussion

5.1. Smoke layer distribution characteristics

Fig. 10 shows the smoke dispersion for different longitudinal ventilation activation times and door openings at steady dispersion $Q = 2$ MW, $V_l = 2.8$ m/s and X^*=0.5. The longitudinal ventilation activation time has no significant influence on the smoke back-layering length, as shown in Fig. 10(a) and 10(b). In both cases, the smoke flows back at 220 s, and the smoke layer stabilizes after 400 s. Fig. 10(a) and Fig. 10(c) show the effect of the door openings on the smoke spread. The comparisons between the different door openings show that the smoke back-layering length is significantly affected by the door opening. The opening of the side doors will result in a shorter smoke back-layering length in the train.

5.2. Critical velocity and confinement velocity models for side door-closed condition

The dimensionless smoke back-layering length obtained from the simulations was then integrated, as illustrated in Fig. 11. Meanwhile, with a correlation value of 0.97, all of the data be connected into a universal form:

$$L^* = 38.2\ln\left(\frac{Q^{*1/3}}{V^*_{\text{in}}}\right) - 7.38 \tag{17}$$

Taking L as zero we can derive the critical train ventilation velocity when the side doors are closed:

$$V^*_{\text{in-c}} = 0.82Q^{*1/3} \tag{18}$$

Recently, many researchers have studied the critical velocity under different fire scenarios in the longitudinal ventilation tunnel (Wu and Bakar, 2000b; Ying et al., 2011; Zhu et al., 2017). The critical velocity is different with various fire scenarios. The value of dimensionless critical velocity is about 0.64 to 1.01 in most fire scenarios according to statistics. The critical train ventilation velocities in this investigation were compared to prediction models for conventional single tunnels, as shown in Fig. 12. It can be seen that the result is similar to the predicted by Ying et al. (2011), and the result is within the reference range of previous studies which further demonstrated the applicability of Eq. (9).

Substituting Eq. (9) into Eq. (18), the expression of the dimensionless critical velocity and the dimensionless fire source power is obtained:

$$V^*_c = 1.03Q^{*1/3} \tag{19}$$

According to Eq. (17), Taking L as L_f we can derive the confinement train ventilation velocity when the side doors are closed:

$$V^*_{\text{in-conf}} = e^{-\left(\frac{L_f}{123}+0.193\right)}Q^{*1/3} \tag{20}$$

We noticed in Eq. (20) that the fire location was considered in the confinement velocity model, unlike the critical velocity model. Different fire location calls for different smoke back-layering length to reach the front of the train. Substituting Eqs. (9), (11) into Eq. (20), the expression of the dimensionless confinement velocity model is obtained:

$$V^*_{\text{conf}} = 1.25e^{-(0.98X^*+0.193)}Q^{*1/3} \tag{21}$$

5.3. Critical velocity and confinement velocity models for side door-opened conditions

While the side doors are opened, the smoke exhaust is influenced by the additive effect of the side doors combines with the train ventilation velocity caused by the pressure difference between the train and the blockage region. Correspondingly, a shorter smoke back-layering length in the train might be generated. Fig. 13 depicts the dimensionless smoke back-layering length in the train with the dimensionless fire location under longitudinal ventilation. Overall, the figure clearly illustrates that L* fluctuate strongly as a logarithmic function of different $Q^{*1/3}/V_l$* at different fire location, and the dimensionless smoke back-layering length in the train steadily decreases as the longitudinal ventilation rate in the tunnel increases.

As a result, the dimensionless critical velocity is obtained by setting the dimensionless back layer length in Fig. 13 to zero, as illustrated in Fig. 14. With the same fire heat release rate, the dimensionless critical velocity decreased firstly and then increased with the increase of the dimension-less fire locations in the train. Near the front of the train (X^*<0.33), the downtrend was caused by the increased number of upstream side doors, which increased the air velocity in the train. Near the rear of the train (X^*>0.67), the uptrend was caused by the decreased number of the downstream side doors, which lowers the smoke exhaust level at the downstream side doors and increases the requirement of airflow inertia force for confining smoke in the train. In the middle of the

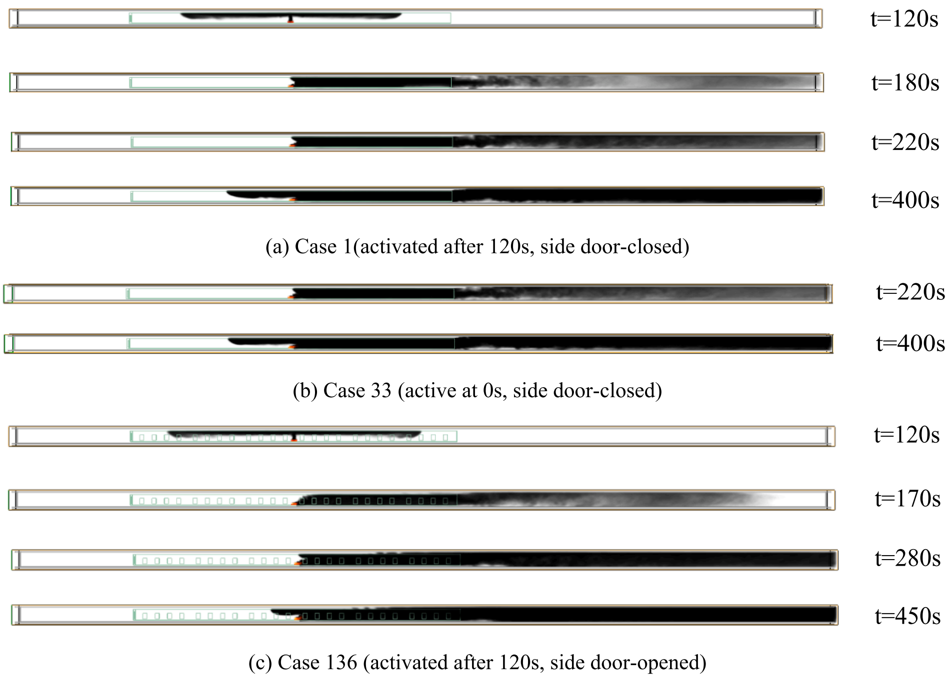

Fig. 10. Smoke spread of various longitudinal ventilation activated time and door opening ways with $Q = 2$ MW, $V_l = 2.8$ m/s, X^*=0.5.

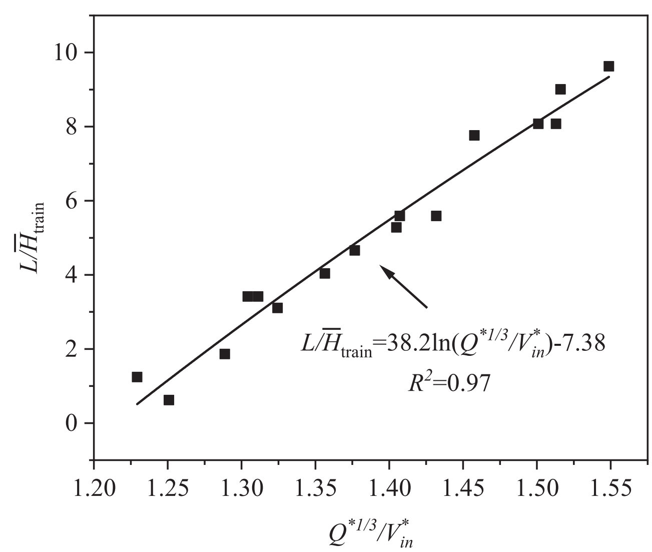

Fig. 11. Relationship between L^* and $Q^{*1/3}/V_{\text{in}}{}^*$ in the train with side door closed.

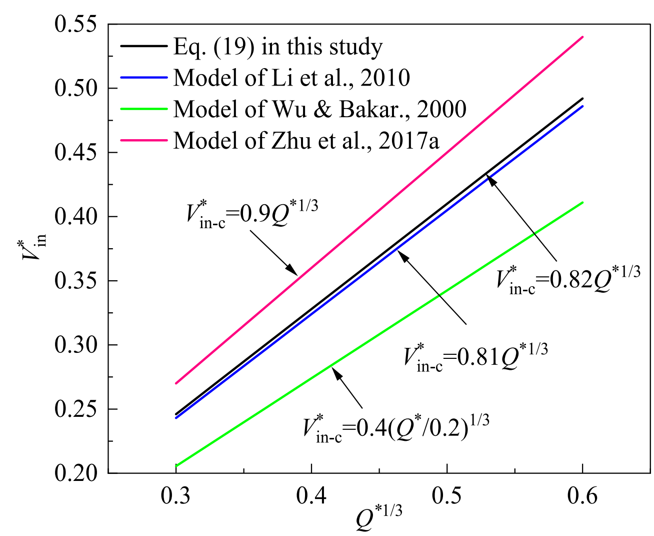

Fig. 12. Comparison between current model (Eq. (18)) and previous models for predicting critical velocity.

train (0.33 ≤ X^*≤0.67), the dimensionless critical velocity stayed almost stable. This was caused by a certain balance achieved between the increase in velocity by the increasing number of the upstream side doors and the increase in airflow inertia force for confining smoke by the decreased number of the downstream side doors. The comparison indicates that the opening of the side doors has a significant effect on smoke control and the V^*_c was, overall, lower than the dimensionless critical velocity model, Eq. (19), for side door-closed.

The smoke flow process and the critical velocity were shown to be significantly influenced by the door openings and longitudinal ventilation, which were indispensable factors of the evacuation option and ventilation mode to consider for smoke control design in underground tunnels. Accordingly, Fig. 15 shows the variation of the dimensionless critical velocity ratio of $V^*_c/\ V^*_c(X^*{=}0.5)$ with a dimensionless fire location. The prediction for $V^*_c/\ V^*_c(X^*{=}0.5)$ can be determined as:

$$\frac{V_c^*}{V_c^*(X^*=0.5)} = 9.8 - 8.8e^{-0.16(X^*-0.53)^2} \tag{22}$$

Therefore, the dimensionless critical velocity for side doors opened can be deduced:

$$\begin{aligned} V_c^* &= 0.76\left[9.8 - 8.8e^{-0.16(X^*-0.53)^2}\right]Q^{*1/3} \\ &= \left[7.45 - 6.69e^{-0.16(X^*-0.53)^2}\right]Q^{*1/3} \end{aligned} \tag{23}$$

With the side doors open, Eq. (23) can be used to calculate the critical velocity by taking the varying fire position into account.

Similarly, the confinement model can be determined by the above method in section 5.2. The dimensionless confinement velocity can be obtained by taking the dimensionless back-layering length as L_f, as shown in Fig. 16. Overall, the confinement velocity in the tunnel was

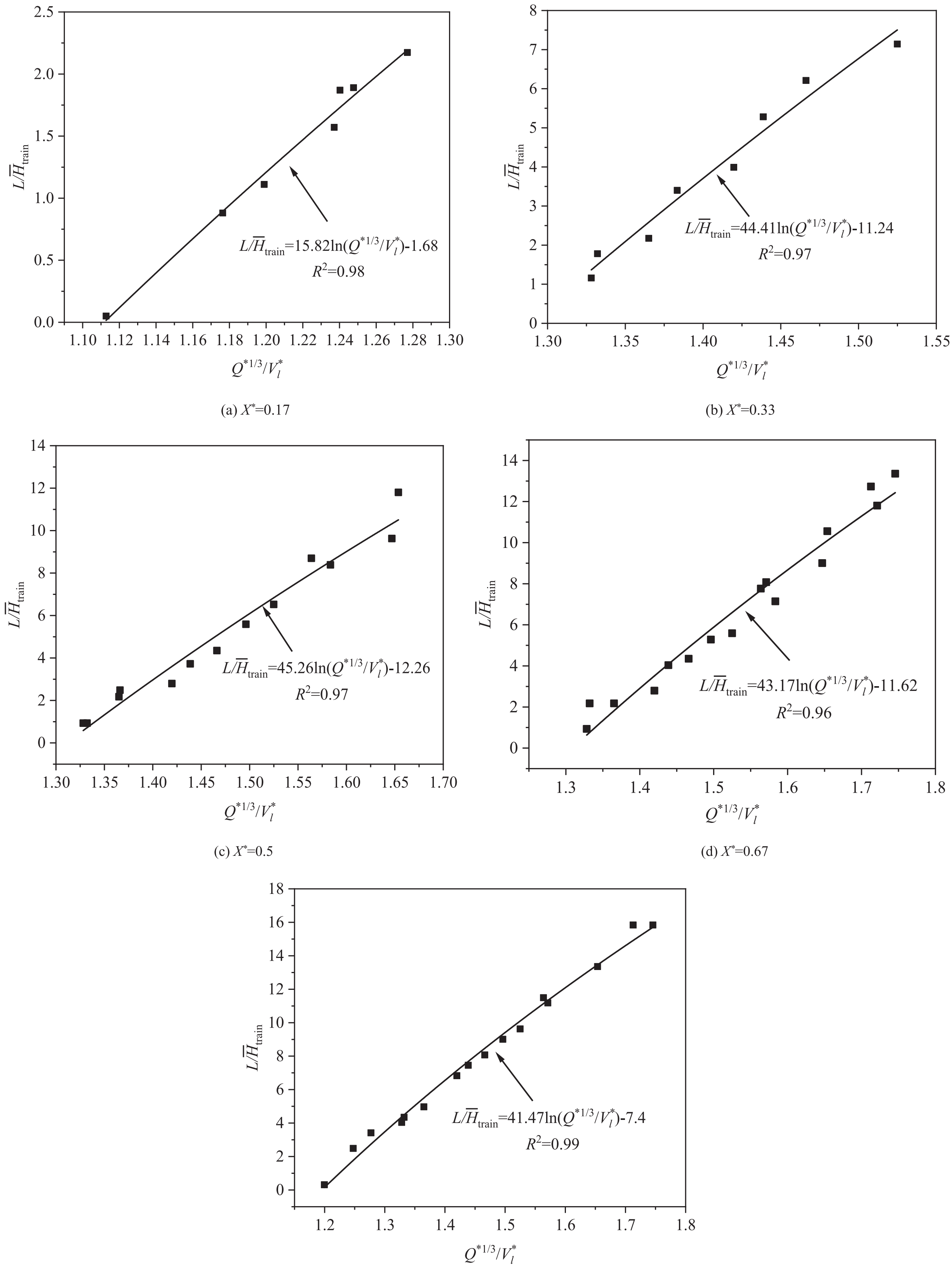

Fig. 13. Comparison between L^* and $Q^{*1/3}/V_l^*$ for different dimensionless fire locations.

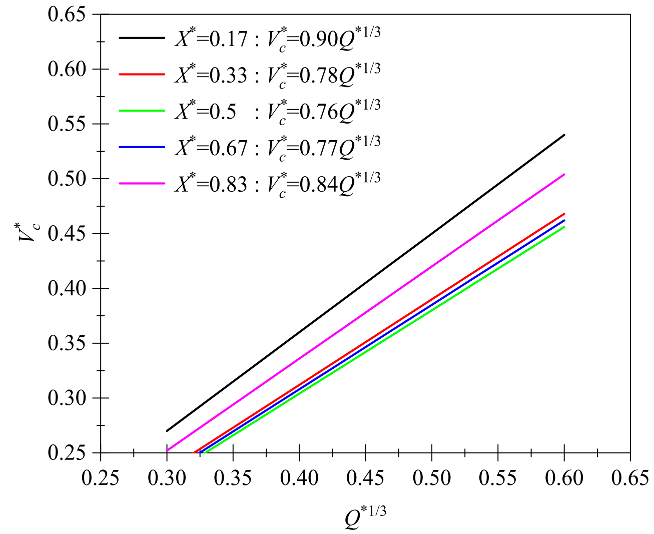

Fig. 14. Dimension-less critical velocity for different fire locations in the train.

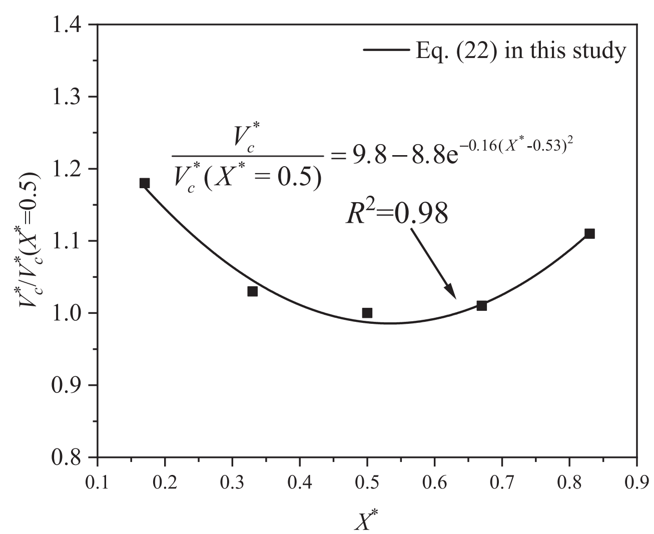

Fig. 15. Effect of the fire location on $V^*_c/V^*_c(X^*=0.5)$.

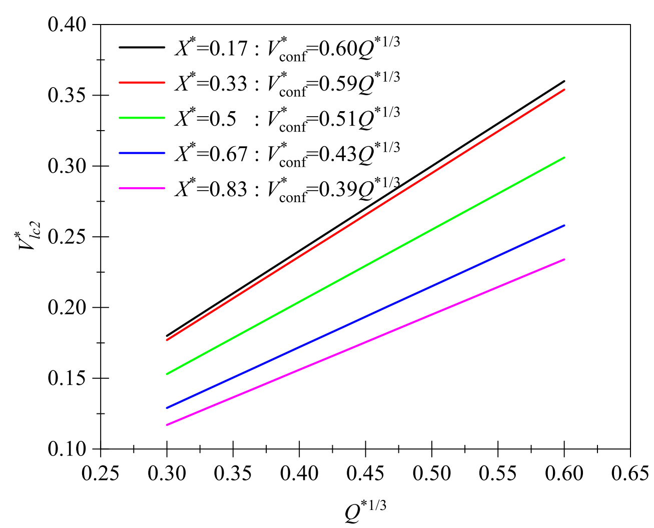

Fig. 16. Dimensionless confinement velocity for different fire locations in the train.

smaller with a long distance from the fire location to the front of the train. The non-dimensional fire position in the train is shown in Fig. 17, along with the confinement ventilation ratio of $V^*_{conf}/\ V^*_{conf}(X^*=0.5)$ which correlate well with each other, and can be expressed as:

$$\frac{V^*_{\mathrm{conf}}}{V^*_{\mathrm{conf}}(X^*=0.5)} = 0.79 + 1.07e^{-4.35X^*} \tag{24}$$

Therefore, the dimensionless confinement velocity for side doors opened can be deduced:

$$\begin{aligned} V^*_{\mathrm{conf}} &= 0.51\left[0.79 + 1.07e^{-4.35X^*}\right]Q^{*1/3} \\ &= \left(0.41 + 0.55e^{-4.35X^*}\right)Q^{*1/3} \end{aligned} \tag{25}$$

5.4. The critical velocity and confinement velocity predicted model

The predicted model for critical velocity and confinement velocity under the different door openings were proposed, respectively. The critical velocity is the longitudinal air speed that completely blows the smoke to the downstream area of the fire source in the compartment. The confinement velocity is the longitudinal air speed that controls the smoke in the downstream area of the train head. Considering that the smoke back-layering length equals zero or the distance from the fire location to the train head, the ventilation velocity can be expressed as Eq. (26) and Eq. (27), respectively.

$$V^*_c = \begin{cases} 1.03Q^{*1/3} & \text{, Side} - \text{door closed} \\ \left[7.45 - 6.69\mathrm{e}^{-0.16(X^*-0.53)^2}\right]Q^{*1/3} & \text{, Side} - \text{door opened} \end{cases} \tag{26}$$

$$V^*_{\mathrm{conf}} = \begin{cases} 1.25\mathrm{e}^{-(0.98X^*+0.193)}Q^{*1/3}, & -\text{door closed} \\ \left(0.41 + 0.55\mathrm{e}^{-4.35X^*}\right)Q^{*1/3}, & \text{Side} - \text{door opened} \end{cases} \tag{27}$$

Under side door-closed condition, the train can be regarded as a tunnel with a single exit and inlet, and the previous research on critical velocity is still applicable to it. The relationship between the longitudinal ventilation velocity V_l and the train ventilation velocity V_{in} can be calculated by Eq. (9). In the process of calculating the confinement velocity, the smoke back-layering length is different with the location of the fire source. The dimensionless fire location is small, the smoke back-layering length has a much smaller request also, magnitude of confinement velocity also smaller. Under side door-opened condition, the increase of train ventilation velocity and the smoke exhaust level at the side doors will decrease the need of critical velocity and confinement velocity under the same HRR. The critical velocity is decreased and then increased with the increase of dimensionless fire location X^*. This was

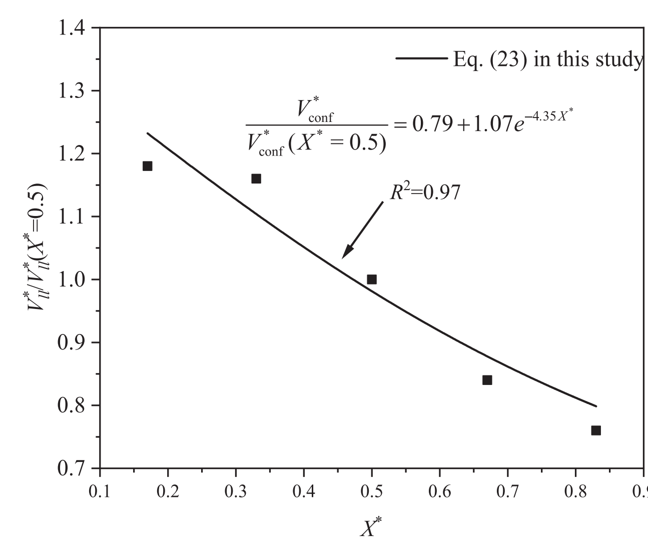

Fig. 17. Effect of the fire location on $V^*_{conf}/V^*_{conf}(X^*=0.5)$.

caused by the imbalance between the increase in velocity by the increasing number of the upstream side doors and the increase in airflow inertia force for confining smoke by the decreased number of the downstream side doors. However, in the process of calculating the confinement velocity. As the dimensionless fire location X^* increased, the increase of train ventilation velocity V_{in} and the decrease of smoke exhaust effect of the side doors have no obvious effect compared to the increase of smoke back-layering length L.

The predictions of critical velocity and confinement velocity calculated by Eq. (26) and Eq. (27) are compared with experimental results, as shown in Fig. 18. It can be seen the predicted values are in good agreement with experimental results under the different door opening ways, indicating that Eq. (26) and Eq. (27) can predict dimensionless critical velocity and confinement velocity induced by train fires in ventilation tunnel for given fire heat release rates within a margined error of 20 %.

5.5. Comparison with other predicted models

There is no any prediction model with a fire location parameter to predict critical velocity and confinement velocity in the underground train fire proposed before. The closely related prediction critical velocity model given by Hu et al. (2020) was selected for comparison to verify the applicability of the current results since the fire scenario in Hu's research is the most similar to this study. The similarities between the two studies were primarily that, first, the experimental model of Hu et al. (2020) consisted of a tunnel and a train with a similar structure to the current model; second, the effect of the side doors was similarly considered when predicting the critical velocity. Notably, the primary differences were that the smoke back-layering length in Hu's study was in the tunnel, while the smoke back-layering length in this study was in the train. Furthermore, Hu et al. (2020) only addressed the influence of one side door in the development of a prediction model, and 24 side doors were simplified into one.

Fig. 19 presents the comparison of Hu's model and the current model with different door opening ways. The fire was located in the middle of the train (X^*=0.5). The results show that the models predicted in this study were always lower than Hu's model. That was attributed to the opening of the emergency evacuation doors. The opening of the emergency evacuation doors can generate greater air pressure in the train. Additionally, as seen in Fig. 20, Hu's model prediction and current results $V^*/Q^{*1/3}$ findings with various fire locations were compared. It is noticed that, Under the same heat release rate, the dimensionless critical

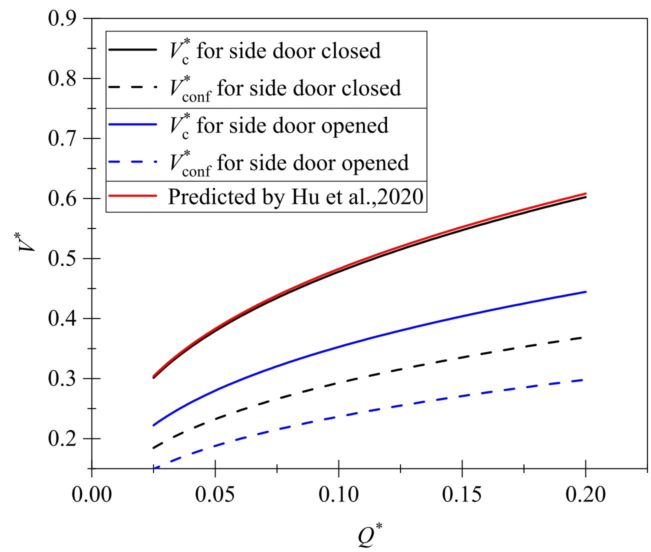

Fig. 19. Comparison between results from current and a previous study considering heat release rate.

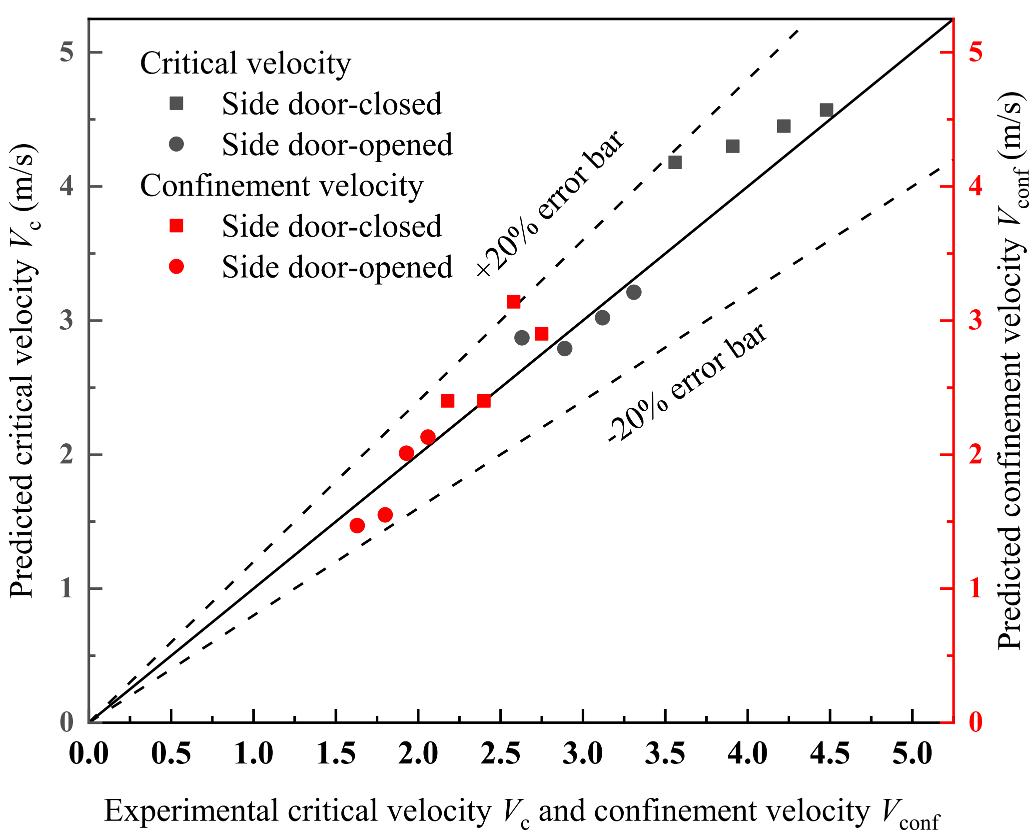

Fig. 18. Comparison of model-predicted values and experimental values.

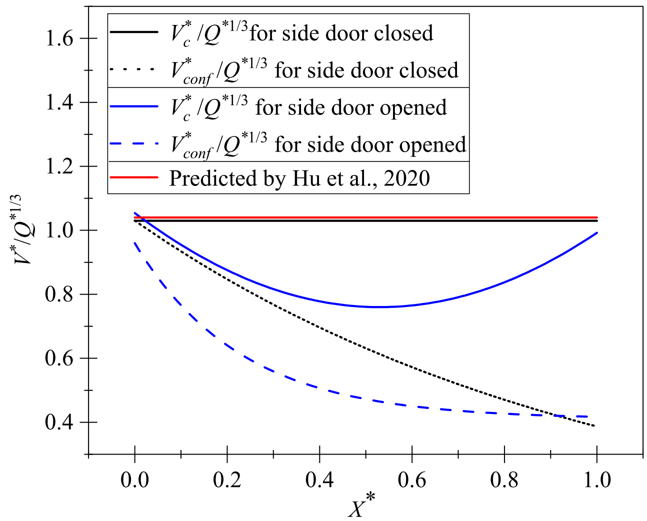

Fig. 20. Comparison between results from current and a previous study considering fire location.

velocity and confinement velocity vary closely with the position of the fire; second, the present model and Hu's model agree well when the fire occurs at the front of the train.

6. Conclusions

Experiments and numerical simulations were conducted to investigate the smoke control induced by train fires in an underground tunnel with different door openings. As for longitudinal ventilation, the critical velocity and confinement velocity models were considered. A series of experimental and simulation tests were conducted by changing the longitudinal ventilation velocity, the fire heat release rates, and the fire source location. The major conclusions are as follows:

(1) For the smoke control for fire environments induced by train fires in a ventilation tunnel, the opening of the side doors would result in a shorter smoke back-layering length in the train. Furthermore, the smoke back-layering length in the train is little influenced by the activation time of the longitudinal ventilation system.
(2) The dimensionless model of the train ventilation velocity and the longitudinal ventilation velocity was developed by theoretical analysis model, and the accuracy was verified by scaled experiments model and numerical simulations. The formula is a universal approach to calculate impingement ventilation in underground tunnels. As we calculate in this paper, the impingement ventilation in the theoretical model assumes that the air direction is perpendicular to the front of the train.
(3) Taking the effect of the door opening ways into account, the prediction models of critical velocity and confinement velocity for confining smoke in an underground tunnel were developed. The model can be applied in the actual smoke control design of underground tunnels with heat release rates of 2–5 MW ($0.09 < Q^* < 0.23$).

The results of this study could provide reference for the fire rescue of stopped subway trains with fire and the formulation of personnel evacuation plans. It should be pointed out that the tunnel ventilation scheme, opening conditions of the side doors and the transverse position of the train fire will all affect the critical velocity and the confinement velocity. Therefore, the results obtained are only applicable to the scenes with longitudinal ventilation, multiple openings on one side and fire located at the longitudinal centerline. At the same time, our current research was carried out without considering the evacuation of people in the train. The activating time of the longitudinal ventilation system did not fully consider whether the evacuated people could be completely in a safe state. In the future, it is necessary to consider the factors of safe evacuation in this double narrow and long space in order to control smoke of train fire effectively.

CRediT authorship contribution statement

Zhihe Su: Methodology, Investigation, Writing – original draft. **Yanfeng Li:** Conceptualization, Supervision, Funding acquisition. **Shan Feng:** Software, Investigation. **Hua Zhong:** Writing – review & editing. **Junmei Li:** Writing – review & editing, Supervision. **Wenbo Liuv:** Investigation. **Chao Chen:** Software. **Jiaxin Li:** Investigation.

Declaration of Competing Interest

The authors declare that they have no known competing financial interests or personal relationships that could have appeared to influence the work reported in this paper.

Data availability

No data was used for the research described in the article.

Acknowledgements

This work was supported by the Beijing Natural Science Foundation (Grant No: 8172006) and the Natural Science Foundation of China (Grant No: 51378040). We sincerely appreciate this support.

Appendix A. Uncertainty analysis

The uncertainty of experimental results depends on the accuracy of experimental equipment. Previous study (Kline and Mcclintock, 1953) discovered that the uncertainty in the calculation results could be estimated with good accuracy on the basis of the root-sum-square (RSS). By combining the uncertainty generated from each variable, the basic equation is expressed as:

$$\delta R = \left(\sum_{i=1}^{N} \left(\frac{\partial R}{\partial X_i} \delta X_i \right)^2 \right)^{1/2} \tag{A1}$$

where each term represents the contribution of one variable's uncertainty, δX_i, to the overall uncertainty in the outcome, δR.

Thereafter, the measurement uncertainty in the current study could be estimate as follows.

(1) Uncertainty of the burning rate measurement.

The previous study (Han et al., 2021; Mofat, 1988) has shown that the relative uncertainty of measured burning rate, $\frac{\delta \dot{m}'}{\dot{m}'}$, can be obtained as:

$$\frac{\delta \dot{m}}{\dot{m}} = \pm\left[\left(\frac{\partial \dot{m}}{\partial \Delta m}\frac{\delta \Delta m}{\Delta m}\frac{\Delta m}{\dot{m}}\right)^2 + \left(\frac{\partial \dot{m}}{\partial \Delta t}\frac{\delta \Delta t}{\Delta t}\frac{\Delta t}{\dot{m}}\right)^2 + \left(\frac{\partial \dot{m}}{\partial A}\frac{\delta A}{A}\frac{A}{\dot{m}}\right)^2\right]^{1/2} \tag{A2}$$

where $\frac{\delta \Delta m}{\Delta m}$, $\frac{\delta \Delta t}{\Delta t}$ and $\frac{\delta A}{\Delta A}$ are respectively represent the relative uncertainties of the measured mass loss, time interval of stable stage, and pool surface area. The uncertainty of fuel quality measurement is mainly determined by the readability, linearity and repeatability of mass flowmeter. Referred to the technical guide, the relative error of all values are ±0.1g. At the same time, the measurement time interval uncertainty of mass flowmeter is 0.5s, and the area of fuel pans is determined by a ruler with uncertainty of 1mm. Substituting these values into Eq. (A2), the maximum relatively uncertainty of the burning rate in this study is less than ±5%.

(2) Uncertainty of the temperature measurement.

In this study, all the combustion tests were carried out under the ambient temperature around 22 °C. At the same time, K-type thermocouple with uncertainty of temperature reading is ± 0.1 °C was used to measure the temperature. Considering a conservative value of ±1°C, the relative uncertainty of temperature is calculated as $\frac{\delta T}{T} = \pm\left(\frac{\pm 1^{\circ} C}{T^{\circ} C}\right)$, the maximum relative uncertainty of temperature measurement is about ± 4.5%.

(3) Uncertainty of the velocity measurement

The arithmetic mean value of nine measuring points is taken as the average velocity of the measuring plane. The uncertainty of $\_u\_u_0$ can be calculated as (Lu et al., 2022):

$$U_{\overline{u_0}} = \sqrt{\sum_{i=1}^{5}\left(\frac{\partial \overline{u_0}}{\partial u_i}U_{u_i}\right)^2} \tag{A3}$$

$$u_i = \frac{1}{n}\sum_{j=1}^{n} u_{i,j} \tag{A4}$$

where $u_{i,j}$ means the j th measured value of u_i, and n is the number of measurements of the i th measuring point. The maximum uncertainty of the velocity in this study is 1.8×10^{-2}, and the maximum uncertainty in Test 17 is ±4.7%.

References

Cong, W., Shi, L., Shi, Z., Peng, M., Cheng, X.J.T., Technology, U.S., 2020. Effect of train fire location on maximum smoke temperature beneath the subway tunnel ceiling. Tunn. Undergr. Space Technol. 97, 103282-.

Du, T., Yang, D., Ding, Y.J.T., Technology, U.S., 2018. Driving force for preventing smoke backlayering in downhill tunnel fires using forced longitudinal ventilation. Tunn. Undergr. Space Technol. 79, 76–82.

Feng, S., Li, Y., Hou, Y., Li, J., Huang, Y.J.T., Technology, U.S., 2020. Study on the critical velocity for smoke control in a subway tunnel cross-passage. Tunn. Undergr. Space Technol. 97, 103234.

Han, J., Geng, P., Wang, Z., Wang, F., Weng, M., L, F., 2021. Effects of fire-blockage distance on pool fire burning behavior and thermal temperature profiles in a naturally ventilated tunnel. Tunn. Undergr. Space Technol. 117, 104131.

Hu, P., Zhang, Z., Zhang, X., Tang, F.J.T., Technology, U.S., 2020. An experimental study on the transition velocity and smoke back-layering length induced by carriage fire in a ventilated tunnel. Tunn. Undergr. Space Technol. 106, 103609.

Huang, Y., Li, Y., Li, J., Li, J., Li, H.J.T., Technology, U.S., 2020. Modelling and experimental investigation of critical velocity and driving force for preventing smoke backlayering in a branched tunnel fire. Tunn. Undergr. Space Technol. 99, 103388.

Ji, J., Gao, Z.H., Fan, C.G., Zhong, W., Heat, J.H.S.J.I.J.o., Transfer, M., 2012. A study of the effect of plug-holing and boundary layer separation on natural ventilation with vertical shaft in urban road tunnel fires. Int. J. Heat Mass Transfer 55, 6032-6041.

Ji, J., Gao, Z.H., Fan, C.G., Sun, J.H., 2013. Large Eddy Simulation of stack effect on natural smoke exhausting effect in urban road tunnel fires. Int. J. Heat Mass Transfer 66, 531–542.

Jiang, X., Zhang, H., Jing, A.J.T., Technology, U.S., 2018. Effect of blockage ratio on critical velocity in tunnel model fire tests. Tunn. Undergr. Space Technol. 82, 584–591.

Ko, G.H., Kim, S.R., Hong, S.R.J.J.o.F.S., 2010. An Experimental Study on the Effect of Slope on the Critical Velocity in Tunnel Fires. J. Fire Sci. 28, 27-47.

Kline, S.J., Mcclintock, F.A., 1953. Describing Uncertainties in Single-Sample Experiments. Mechanical engineering 1919, 75.

Li, Y.Z., Ingason, H.J.F.S.J., 2017. Effect of cross section on critical velocity in longitudinally ventilated tunnel fires. Fire Saf. J. 91, 303–311.

Li, Y.Z., Ingason, H.J.T., Technology, U.S., 2018. Overview of research on fire safety in underground road and railway tunnels. Tunn. Undergr. Space Technol. 81, 568–589.

Li, J., Li, Y.F., Cheng, C.H., Chow, W.K.J.T., Technology, U.S., 2019. A study on the effects of the slope on the critical velocity for longitudinal ventilation in tilted tunnels. Tunn. Undergr. Space Technol. 89, 262–267.

Liu, C., Zhong, M., Song, S., Xia, F., Long, Z.J.T., Technology, U.S., 2020. Experimental and numerical study on critical ventilation velocity for confining fire smoke in metro connected tunnel. Tunn. Undergr. Space Technol. 97, 103296.

Lu., X., Weng., M., Liu., F., Wang., F., Han., J., Chipok., C., 2022. Effect of bifurcation angle and fire location on smoke temperature profile in longitudinal ventilated bifurcated tunnel fires. Tunn. Undergr. Space Technol. 127, 104610.

Marková, I., Lauko, J., Makovická Osvaldová, L., Mózer, V., Svetlík, J., Monoši, M., Orinčák, M., 2020. Fire size of gasoline pool fires. Int. J. Environ. Res. Public Health 17 (2), 411.

Mcgrattan, K., Forney, G., Floyd, J.E., Hostikka, S., Prasad, K., 2010. Fire Dynamics Simulator (Version 4) User's Guide.

Mofat, R.J., 1988. Describing the uncertainties in experimental results. Exp. Therm Fluid Sci. 1, 3–17.

Oka, Y., Atkinson, G.T., 1995. Control of smoke flow in tunnel fires. Fire Saf. J. 25, 305–322.

Peng, M., Shi, L., He, K., Yang, H., Richard, Y.J.F.T., 2019. Experimental study on fire plume characteristics in a subway carriage with doors. Fire Technol.

Shafee, S., Yozgatligil, A.J.T., Technology, U.S., 2018. An analysis of tunnel fire characteristics under the effects of vehicular blockage and tunnel inclination. Tunn. Undergr. Space Technol. 79, 274–285.

Tang, W., Hu, L.H., Chen, L.F., 2013. Effect of blockage-fire distance on buoyancy driven back-layering length and critical velocity in a tunnel: An experimental investigation and global correlations. Appl. Therm. Eng. 60, 7–14.

Thomas, P.H., 1958. The movement of buoyant fluid against a stream and venting of underground fires. Fire Saf. J. 351. -1–1.

Vauquelin, O., Telle, D.J., 2005. Definition and experimental evaluation of the smoke "confinement velocity" in tunnel fires. Fire Saf. J. 40, 320–330.

Weng, M.C., Lu, X.L., Liu, F., Shi, X.P., Yu, L.X.J.T., Research, U.S. 2015. Prediction of backlayering length and critical velocity in metro tunnel fires. Tunn. Undergr. Space Technol. 47, 64-72.

Wu, Y., Bakar, M.Z.A., 2000. Control of smoke flow in tunnel fires using longitudinal ventilation systems – a study of the critical velocity. Fire Saf. J. 35, 363–390.

Yan, F.W., Pei, N.Y., Zhang, B., Jiang, J.C., 2016. Thermal buoyant smoke back-layering length in a naturally ventilated tunnel with vertical shafts. Appl. Therm. Eng. 93, 947–957.

Yao, Y., Cheng, X., Zhang, S., Zhu, K., Shi, L., Zhang, H.J., 2016. Smoke back-layering flow length in longitudinal ventilated tunnel fires with vertical shaft in the upstream. Appl. Therm. Eng. 107, 738–746.

Ying, Z.L., Bo, L., Ingason, H., 2011. Study of critical velocity and backlayering length in longitudinally ventilated tunnel fires. Fire Saf. J. 45, 361–370.

Zhang, S., Yao, Y., Zhu, K., Li, K., Zhang, R., Lu, S., Cheng, X.J.T., Research, U.S., 2016. Prediction of smoke back-layering length under different longitudinal ventilations in the subway tunnel with metro train. Tunn. Undergr. Space Technol. 53, 13-21.

Zhao, S., Liu, F., Wang, F., Weng, M., Zeng, Z.J.T., Technology, U.S., 2018. A numerical study on smoke movement in a metro tunnel with a non-axisymmetric cross-section. Tunn. Undergr. Space Technol. 73, 187–202.

Zhou, Y., Bi, H., Wang, H., Lei, B.J.T., technology, u.s., 2019. Critical velocity in the transverse passages of a railway tunnel rescue station with semi-transverse ventilation. Tunn. Undergr. Space Technol. 92, 103064.103061-103064.103011.

Zhu, K., Shi, L., Yao, Y., Zhang, S., Cheng, X.J.F.T., 2017. Smoke Movement in a Sloping Subway Tunnel Under Longitudinal Ventilation with Blockage. Fire Technol. 1–22.